DOI: 10.1002/chem.200801003

# Effect of the Nature of the Metal Atom on Hydrogen Bonding and Proton Transfer to [Cp*$MH_3$(dppe)]: Tungsten versus Molybdenum**

**Natalia V. Belkova,[a] Maria Besora,[b] Miguel Baya,[c] Pavel A. Dub,[a] Lina M. Epstein,[a] Agustí Lledós,*[b] Rinaldo Poli,[c] Pavel O. Revin,[a] and Elena S. Shubina*[a]**

**Abstract:** The hydrogen-bonding and proton-transfer pathway to complex [Cp*W(dppe)$H_3$] (Cp* = $\eta^5$-$C_5Me_5$; dppe = $Ph_2PCH_2CH_2PPh_2$) was investigated experimentally by IR, NMR, UV/Vis spectroscopy in the presence of fluorinated alcohols, *p*-nitrophenol, and $HBF_4$, and by using DFT calculations for the [CpW(dhpe)$H_3$] model (Cp = $\eta^5$-$C_5H_5$; dhpe = $H_2PCH_2CH_2PH_2$) and for the real system. A study of the interaction with weak acids ($CH_2FCH_2OH$, $CF_3CH_2OH$, $(CF_3)_2CHOH$) allowed the determination of the basicity factor, $E_j = 1.73 \pm 0.01$, making this compound the most basic hydride complex reported to date. A computational investigation revealed several minima for the [CpW(dhpe)$H_3$] adducts with $CF_3CH_2OH$, $(CF_3)_2CHOH$, and $2(CF_3)_2CHOH$ and confirms that these interactions are stronger than those established by the Mo analogue. Their geometries and relative energies are closely related to those of the homologous Mo systems, with the most stable adducts corresponding to H bonding with M–H sites, however, the geometric and electronic parameters reveal that the metal center plays a greater role in the tungsten systems. Proton-transfer equilibria are observed with the weaker proton donors, the proton-transfer step for the system [Cp*W(dppe)$H_3$]/$HOCH(CF_3)_2$ in toluene having $\Delta H = (-3.9 \pm 0.3)$ kcal mol$^{-1}$ and $\Delta S = (-17 \pm 2)$ cal mol$^{-1}$ K$^{-1}$. The thermodynamic stability of the proton-transfer product is greater for W than for Mo. Contrary to the Mo system, the protonation of the [Cp*W(dppe)$H_3$] appears to involve a direct proton transfer to the metal center without a nonclassical intermediate, although assistance is provided by a hydride ligand in the transition state.

**Keywords:** hydrido complexes · hydrogen bonds · phosphine ligands · proton transfer · tungsten

## Introduction

Hydrogen bonds involving transition-metal mono- and polyhydrides as proton acceptors have attracted considerable attention in recent years due to their involvement in intermediates of fundamental processes such as enzymatic dihydrogen evolution and catalytic ionic hydrogenation.[1–6] As proton acceptors, M–H moieties offer a relatively unencumbered site of attack, in which the proton-accepting orbital $\sigma_{MH}$ (mostly constituted by the spherically symmetrical 1s orbital of the H atom)[7] is relatively insensitive to angular limitations for the best interaction with the proton donor (Figure 1a). Spectroscopic manifestations of hydrogen bonding in (M)–H···H–A complexes are similar to those found in the case of classical hydrogen bonding.[8] Accordingly, the

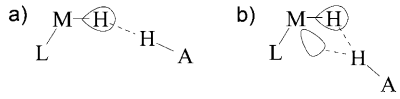


Figure 1. Possibilities for the metal hydride interaction with proton donors.

[a] Dr. N. V. Belkova, P. A. Dub, Prof. Dr. L. M. Epstein, Dr. P. O. Revin, Prof. Dr. E. S. Shubina
A. N. Nesmeyanov Institute of Organoelement Compounds
RAS, Vavilov Street 28, 119991 Moscow (Russia)
Fax: (+7) 499-135-5085
E-mail: shu@ineos.ac.ru

[b] Dr. M. Besora, Prof. Dr. A. Lledós
Departament de Química, Universitat Autónoma de Barcelona
08193 Bellaterra (Spain)
Fax: (+34) 935-812-920
E-mail: agusti@klingon.uab.es

[c] Dr. M. Baya, Prof. Dr. R. Poli
Laboratoire de Chimie de Coordination
UPR CNRS 8241 liée par convention à l'Université Paul Sabatier et à l'Institut National Polytechnique de Toulouse
205 Route de Narbonne, 31077 Toulouse (France)

[**] Cp* = $\eta^5$-$C_5Me_5$; dppe = $Ph_2PCH_2CH_2PPh_2$.

Supporting information for this article is available on the WWW under http://dx.doi.org/10.1002/chem.200801003.

   

(M)H···H-A angles tend to be linear in dihydrogen-bonded complexes.[9] On the other hand, the dihydrogen-bonded complexes of metals with a $d^n$ ($n=2$) configuration (namely, possessing at least one metal-based lone pair) often feature the nonlinear M–H···H(A) arrangement, such that the proton-donor A–H bond approaches the M–H unit in a side-on direction.[10] A typical H···M distance in such a case was found to be 2.8 Å, leading to a possible ambiguity, because a metal's $d_\pi$ nonbonding orbital, if pointing between the ligands, could, in principle, interact with the A–H proton (Figure 1b). Providing the hydrogen bonding involving metal lone pairs as proton acceptors is very well established for metal complexes that do not contain hydride ligands (e.g., $L_nM\cdots HA$ with $L\neq H$),[11–16] this may not only mean an additional interaction, but may ultimately lead to the proton-donor coordination to the metal center. However, many examples are known in which the protonating reagent attacks a hydride position, yielding a dihydrogen complex as the kinetically controlled protonation product, even when the classical di- or polyhydride product is thermodynamically favored.[17–22]

This general behavior for the protonation of hydride complexes may be summarized as shown in Scheme 1, in which the initial competition between a metal lone pair and a hydride unit leads to the hydrogen-bonded adducts **I** and **II**, respectively. In the second case, however, both the hydride ligand and the metal atom could contribute to the interaction, leading to either a dihydrogen complex or a *cis*-dihydride, depending on the relative energy of these isomers. Note that the isomerization process interconverting a dihydrogen complex and a *cis*-dihydride, in cases involving a possible double minimum, is predicted to have a very small activation barrier,[23] whereas much larger activation barriers are associated with processes in which a more severe ligand rearrangement occurs, such as in *cis*/*trans* isomerizations.[24–28]

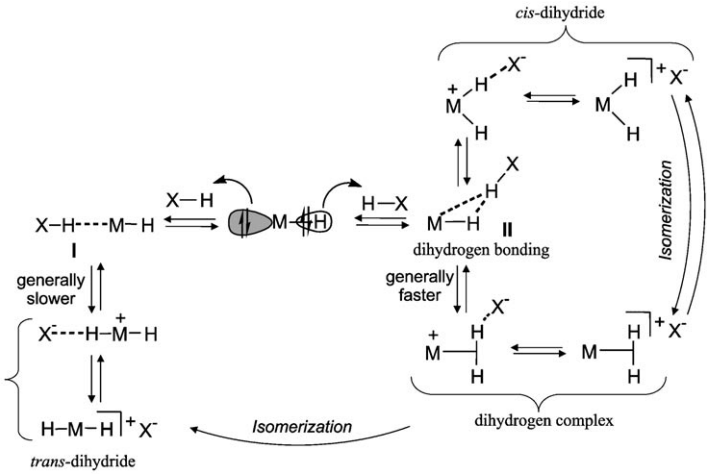


Scheme 1. Two pathways of proton transfer to transition-metal hydrides.

Given the above scenario, it may be reasonable to expect that the kinetic preference for attack at an M–H site versus the metal lone pair should be greater for a polyhydride compound than for a monohydride compound. Recently, we reported detailed investigations[29,30] on the hydrogen bonding and proton transfer to complex $[Cp^*Mo(dppe)H_3]$, an electron-rich half-sandwich trihydride complex of $Mo^{IV}$.[31] The protonation product observed by the use of either strong ($HBF_4$, $CF_3COOH$) or moderate (perfluoro-*tert*-butanol (PFTB), hexafluoroisopropanol (HFIP), *p*-nitrophenol) acids is the classical tetrahydrido derivative, $[Cp^*Mo(dppe)H_4]^+$, without detection of any nonclassical intermediate, even upon working at 200 K. On the other hand, use of even weaker proton donors (2,2,2-trifluoroethanol (TFE), 2-fluoroethanol (MFE)), and low temperatures (200 K), backed up by a theoretical investigation, revealed that the most likely site of attack is a hydride ligand. The calculations, which were carried out in the $[CpMo(dhpe)H_3]$ model system ($dhpe=H_2PCH_2CH_2PH_2$), could also locate the nonclassical protonation product, $[CpMo(dhpe)(\eta^2\text{-}H_2)H_2]^+$, in a shallow energy minimum and showed that its rearrangement to the more stable (by 1.5 kcal mol$^{-1}$ in the gas phase, 1.7 kcal mol$^{-1}$ in $CH_2Cl_2$ solution) classical tetrahydrido product occurs with an extremely small activation barrier of 1.8 kcal mol$^{-1}$ in the gas phase (1.3 kcal mol$^{-1}$ by use of the polarizable continuum model (PCM) in $CH_2Cl_2$).[29] Thus, it appears that this complex undergoes a kinetically favored protonation of a hydride ligand, however, the resulting dihydrogen complex does not accumulate at sufficiently high concentration for detection before rearranging to the final tetrahydrido product.

It is of interest to investigate trends of fundamental properties for series of compounds with the same stoichiometry for metals within the same group. This kind of knowledge for hydrogen bonding and proton transfer to transition-metal hydrides is still scarce, the only two series of hydrides studied to date being $[PP_3MH_2]$ (M = Fe, Ru, Os; $PP_3=P(CH_2CH_2PPh_2)_3$)[32,33] and $[Cp^*MH(dppe)]$ (M = Fe, Ru).[24,25,27] Thus, we have proceeded to investigate the behavior of $[Cp^*W(dppe)H_3]$ hydride[31] in terms of hydrogen bonding and proton transfer. The results of this investigation and a comparison with those previously described for the Mo analogue are reported here.

## Results

The investigation of hydrogen bonding and proton transfer to complex $[Cp^*WH_3(dppe)]$ followed a combined spectroscopic and theoretical protocol, similar to that used previously for complexes $[Cp^*M(dppe)H]$ (M = Fe, Ru),[24,25,27] $[Cp^*Mo(dppe)H_3]$,[29,30] and $[CpRuH(CO)(PCy_3)]$.[34]

**Study of the starting trihydride complex**: The synthesis and full characterization of this compound has been reported previously.[31,35] An X-ray structure was reported for the Mo analogue and the similarity of the spectroscopic properties

  

and chemical behavior leave no reason to suspect that the structure may be different for the W trihydride complex. It must be underlined that [Cp*Mo(dppe)$H_3$] adopts a pseudo-trigonal prismatic structure (once the Cp* ligand is idealized as occupying a single coordination position coinciding with the ring centroid), instead of the much more common pseudo-octahedral arrangement. However, the same geometry has since been observed for other isoelectronic half-sandwich hydride complexes of Group 6 metals, that is, [($C_5HiPr_4$)Mo($PMe_3$)$_2H_3$][36,37] and [WCp*$(CO)_2H_2$-($SiH_2Ph$)].[38] The adoption of the same structure by [Cp*W-(dppe)$H_3$] was also suggested by subsequent DFT geometry optimizations, which were run at the B3LYP/LANL2DZ level, on the smaller [CpW(dhpe)$H_3$] model system in which the methyl groups of the cyclopentadienyl ring and the phenyl rings of the dppe ligand were substituted by hydrogens.[39]

To compare the structure of the trihydride compound with those of the hydrogen-bonded adducts and proton-transfer products, and to analyze the computational results in greater detail, the optimization of the same model complex [CpW$H_3$(dhpe)] was repeated with a more extensive basis set (see Computational Details) and includes the frequency calculations. Furthermore, selected calculations were carried out on the real complex to check the appropriateness of the smaller model. Cartesian coordinates of all optimized geometries are available in the Supporting Information.

As expected, the calculated structural parameters closely match those obtained with the previous calculations and experimentally obtained for the Mo analogue, whereas the spectroscopic parameters resemble those found for the molybdenum congener.[29] A view of the optimized geometry is shown in Figure 2. As is perhaps best appreciated from the top view in Figure 2c, the three hydride ligands are asymmetrically disposed, one on one side and two on the opposite side of the plane that contains the two P donors and the Cp* ring centroid. Atoms H1 and H2, although being situated rather symmetrically across the ideal plane that contains atoms W, H3, and the ring centroid, are not equivalent in terms of the W–H distances and Mulliken charges, H1 being closest to the metal atom and possessing a higher negative charge than H2. The unique H3 atom exhibits the longest W–H distance and bears the highest negative charge, thus clearly appearing as the most hydridic site.

An IR study of complex [Cp*$WH_3$(dppe)] was also previously reported,[39] although the low spectral quality prevented an unambiguous assignment of the three expected normal modes for the $WH_3$ moiety. Therefore, a higher quality spectrum has now been obtained. Like its molybdenum analogue, [Cp*$WH_3$(dppe)] displays a wide $\nu_{MH}$ band of complex shape, which is superimposed with a few weaker features belonging to overtones of the phenyl-group vibrations. A band decomposition, performed after subtraction of the dppe spectrum, shows the presence of three $\nu_{MH}$ vibrations: 1964w, 1882m, 1846s $cm^{-1}$ in THF; 1959w, 1873s, 1822s $cm^{-1}$ in $CH_2Cl_2$ (see Figure S1 in the Supporting Information). These were assigned on the basis of the computation of the W–H normal modes, which are represented schematically in Figure 3. Thus, the higher-energy normal mode

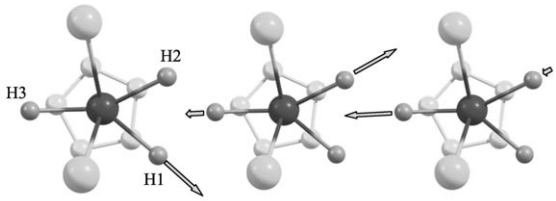


| | $\nu_1$ = 1948 $cm^{-1}$ | $\nu_2$ = 1864 $cm^{-1}$ | $\nu_3$ = 1812 $cm^{-1}$ |
|---|---|---|---|
| *A* | 0.27 | 0.48 | 0.67 |
| W-H1 | ***0.844*** | 0.048 | 0.064 |
| W-H2 | 0.035 | ***0.718*** | 0.186 |
| W-H3 | 0.091 | 0.194 | ***0.672*** |

Figure 3. The W–H normal modes of the DFT optimized [CpW(dhpe)$H_3$] with their frequency, intensity (*A*, $10^4$ $L\,mol^{-1}\,cm^{-2}$), and potential-energy distribution (major components are in bold italic). The Cp- and P-bonded H atoms and ethylene backbone have been omitted for clarity.

($\nu_1$) is essentially a pure stretching vibration of the hydride ligand H1, which shows the shortest (and therefore strongest) bond. The other two vibrations are relatively close to each other in frequency and are a mixture of the other two M−H bond vibrations, the higher-frequency one ($\nu_2$) being an in-phase combination with the major contribution from the shorter bond to H2, and the lower-frequency one ($\nu_3$) being an out-of-phase combination with the major contribution from the longer bond to H3. The intensities of the $\nu_{MH}$ bands increase as the temperature is decreased. The absorbance of the strongest band changes upon cooling from 270 to 200 K from 59.5 to 75.9 $L\,mol^{-1}\,cm^{-1}$ in THF and from 60.5 to 85.5 $L\,mol^{-1}\,cm^{-1}$ in $CH_2Cl_2$.

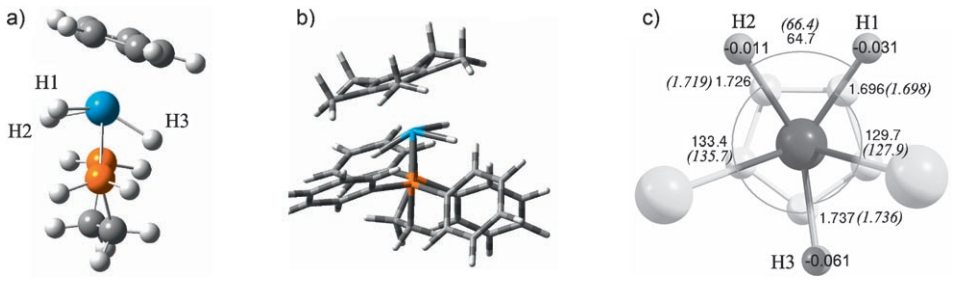


Figure 2. Optimized geometry of a) [CpW(dhpe)$H_3$], b) [Cp*W(dppe)$H_3$], and c) main geometrical parameters (distances in Å, angles in degrees) for the $WH_3$ moiety. The values in parentheses correspond to those optimized for the full system. The numbers on the three H atoms are the computed Mulliken charges.

  

**Hydrogen bonding to [Cp*W(dppe)H$_3$]: Experimental information**: The IR study of the interaction of [Cp*WH$_3$(dppe)] with MFE and TFE in $CH_2Cl_2$, carried out in the $\nu_{OH}$ range, shows the appearance of the expected low-frequency shifted and quite broad $\nu_{OH}$ band for the hydrogen-bonded OH group. It is important to underline that these measurements are carried out with excess hydride, thus favoring the formation of 1:1 adducts. From the analysis of the $\nu_{OH}$ region of the spectrum, the hydrogen-bond enthalpies, $-\Delta H°$, were obtained by two independent methods; the Van't Hoff method (Table 1)[8,40] and the empirical correlation outlined in Equation (1):

$$-\Delta H^\circ = \frac{18\Delta\nu}{\Delta\nu + 720} \quad (1)$$

Subsequent use of the Iogansen relationship[41–43] gives the basicity factor $E_j$ reported in Table 1, making [Cp*WH$_3$(dppe)] the most basic transition-metal hydride compound reported so far.[9] This justifies the observation that even the weakest fluorinated alcohol MFE is sufficiently acidic to afford equilibrium amounts of the proton-transfer product in $CH_2Cl_2$ (see below).

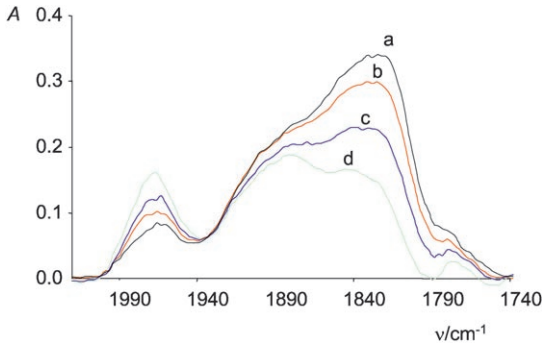


Figure 4. IR spectra of [Cp*W(dppe)H$_3$] (0.04 M) in the $\nu_{W-H}$ stretching region in the presence of MFE at the following concentrations: a) 0 M; b) 0.2 M; c) 0.4 M; d) 0.6 M. $CH_2Cl_2$, 200 K.

Table 1. Parameters of the hydrogen bonding between [Cp*WH$_3$(dppe)] and MFE or TFE, and basicity factors of the hydride complex.

| ROH | $\nu_{OH(free)}$ [cm$^{-1}$] | $\nu_{OH(bonded)}$ [cm$^{-1}$] | $\Delta\nu$ [cm$^{-1}$] | $\Delta\nu_{1/2}$ [cm$^{-1}$] | $\Delta H°$ [a] [kcal mol$^{-1}$] | $\Delta H°$ [b] [kcal mol$^{-1}$] | $\Delta S°$ [b] [cal mol$^{-1}$ K$^{-1}$] | $E_j$ |
|---|---|---|---|---|---|---|---|---|
| MFE[c] | 3608 | 3248 | 360 | 261 | −6.0 | | | 1.74 |
| TFE[c] | 3604 | 3140 | 464 | 251 | −7.1 | −6.5 ± 0.6 | −18 ± 2 | 1.72 |
| HFIP[d] | 3535 | | | | | −7.6 ± 0.9 | −19 ± 3 | 1.77 |

[a] $\Delta H^o$ parameter calculated by the empirical relationship of Equation (1). [b] $\Delta H°$ and $\Delta S°$ parameters calculated by the Van't Hoff method. [c] In $CH_2Cl_2$. [d] In toluene. In this solvent, maximum of $\nu_{OH(bonded)}$ band is masked by $\nu_{CH}$ absorptions.

In an attempt to establish which of the four possible sites, namely the W atom and the three hydride ligands, is used as proton-acceptor site for hydrogen bonding, the IR spectra were analyzed in the $\nu_{MH}$ stretching-vibration region in the presence of proton donors. Following previous studies, dihydrogen bonding (i.e., H bonding to a hydride site) results in a low-frequency shift of the corresponding M–H stretching vibration band, whereas hydrogen bonding to a metal lone pair causes a high-frequency shift.[8,9,40] However, the mixing of bond vibrations in the normal modes for polyhydride compounds makes the analysis of frequency shifts much more complicated. This was clearly demonstrated for the [Cp*MoH$_3$(dppe)]·alcohol system,[29] in which the interaction (excess MFE, $CH_2Cl_2$, 200 K) leads to broadening and to a small ($-5$ cm$^{-1}$) low-frequency shift of the $\nu_{MoH}$ band, attributed to the effect of dihydrogen bonding. For the present compound, similar and even more pronounced spectroscopic changes would be expected, due to the higher basicity of the tungsten hydride complex, if the H bonding site was the same as for the Mo analogue. Instead, a gradual high-frequency shift and an intensity decrease for the major $\nu_{WH}$ band of [Cp*WH$_3$(dppe)] were observed in the presence of increasing amounts of MFE in $CH_2Cl_2$ at 200 K (Figure 4). However, no unambiguous band deconvolution was possible for these spectra because of the occurrence of partial proton transfer, even under these mild conditions. These spectroscopic changes underscore a difference between the nature of the H-bonded adduct for the homologous Mo and W trihydrides complexes, however, the above-mentioned problem of possible M–H vibration mixing in the normal mode requires caution for the extrapolation of these observations to a structural assignment.

Additional experimental evidence was sought by $^1$H and $^{31}$P{$^1$H} NMR spectroscopy using the interaction of [Cp*W(dppe)H$_3$] with HFIP in [D$_8$]toluene. In the absence of proton donor the hydride signal of [Cp*W(dppe)H$_3$] ($\delta$ −5.99, 210 K) exhibits a minimum value of the longitudinal relaxation time $T_{1min}$ of 0.425 s at 250 K (500 MHz). Upon addition of approximately two equivalents of HFIP this signal does not significantly shift and its $T_{1min}$ is only approximately 10% lower (0.391 s at 250 K). A summary of all $T_1$ measurements is available in the Supporting Information (Figure S2). For unambiguous cases of hydrogen bonding to hydrides, an upfield shift and a significant (e.g., 20% or more) lowering of $T_{1min}$ is observed for the hydride resonance, even for polyhydrides. For example, the magnitude of the high-field signal shifts and $T_1$ relaxation-time measurements show preferential coordination of the alcohol to the central hydride of [Cp$_2$NbH$_3$].[44] Similarly, upfield shift and $T_{1min}$ shortening found for one of the two hydride signals of [P(CH$_2$CH$_2$PPh$_2$)$_3$OsH$_2$][32] or [H$_2$Re(CO)(NO)(PMe$_3$)$_2$][45] in the presence of fluorinated alcohols was interpreted as evidence for dihydrogen bonding to the more hydridic hydride ligand. Thus, the NMR data, like the IR data, reported herein do not allow an unambiguous assignment of the H-bonding site. For these reasons, we have turned to a computational investigation of the H-bonding interaction.

  

**Hydrogen bonding to [Cp*W(dppe)H$_3$]: A computational insight**: The formation of hydrogen-bonded adducts was investigated with both TFE and HFIP, using the model [CpW(dhpe)H$_3$] system for most investigations. Because previous studies have shown the importance of the cooperative effect of two proton-donor molecules for the subsequent proton-transfer process, selected calculations were also carried out on bis-alcohol adducts. The evaluation of the interaction energies is subject to the basis set superposition errors (BSSE), especially in cases such as this one in which the interaction is weak and the basis sets used are not very large.[44] The typical counterpoise correction was applied.[46] In addition, the interaction energies were evaluated in dichloromethane solution by running single-point calculations on the gas-phase optimized geometries with the polarizable continuum model (PCM) (Figures 5 and 6).[47,48] For complex **A** (TFE)/**A′** (HFIP), the proton donor interacts with the unique hydride ligand H3. These adducts are those showing the longest distance of the proton from the W atom. For adducts **B**/**B′**, the proton donor is on the other side of the P-W-P plane close to the hydride ligands H1 and H2. It interacts simultaneously with both W–H bonds, more strongly with one of the two (H2 for **B** and **B2′**, H1 for **B1′**), and the separation from the W atom is also relatively short. The O-H···H(W) angles are between 154 and 162°, and the O-H···W angles are in the 160–167° range. Notably, the W···H(O) distance in these adducts is shorter that in the related Mo complexes, thus suggesting the significant participation of the metal atom to H bonding.[29] The **C** (TFE) and **C1′**, **C2′** (HFIP) isomers feature a nearly linear O–H···W moiety (172–177°) and the shortest (O)H···W distances and, thus, the strongest hydrogen bonds with the metal center. The **C2′** isomer also shows a relatively short distance to H3 (1.809) and a relatively wide O-H···H3 angle (142.1°). The main interaction, however, is with the metal center. Thus, it seems that a metal lone pair contributes the most to the interaction in these adducts. Finally, species **D**/**D′** feature very short W-H3···H(O) "dihydrogen bonds". At first glance, they should be considered together with adducts **A**/**A′**. However, an additional interaction with the tungsten atom in **D**/**D′** is evident from the rather short W···H(O) distances and from the wide O–H···W angles, closer to linearity than O–H···H3. Species **C2′** and **D**/**D′** also show a significant tilting of the dhpe ligand toward the Cp ring, relative to free [CpW(dhpe)H$_3$]. Hydrogen-bond formation also leads to an electron-density shift, increasing the absolute value of the negative charge on the hydride ligand and/or tungsten atom involved in the interaction (see Tables 2 and 3).

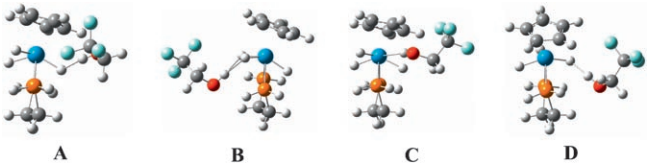


Figure 5. Optimized structures of the [CpW(dhpe)H$_3$]·TFE adducts.

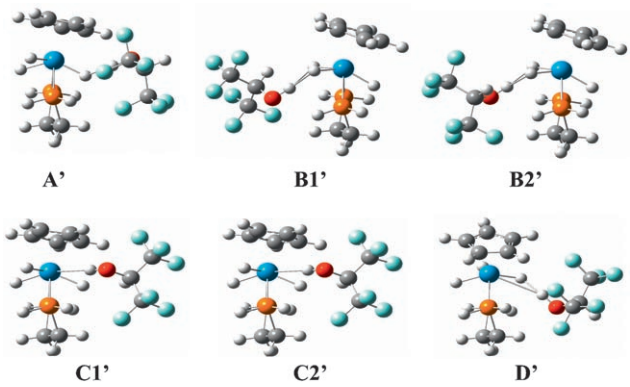


Figure 6. Optimized structures of the [CpW(dhpe)H$_3$]·HFIP adducts.

To gain an insight into the proton-transfer process, which requires the addition of two proton-donor molecules (see section "Kinetics of the proton-transfer process" below), calculations were also carried out on bis-HFIP adducts, still using the smaller [CpW(dhpe)H$_3$] model. Details of these calculations are given in the Supporting Information. As expected,[29,34] the second HFIP molecule further stabilizes energetically the hydrogen-bonded species by stabilizing the partial negative charge on the oxygen atom through the additional hydrogen bond with the second proton-donor molecule. This O–H···O hydrogen bond further strengthens the primary [CpW(dhpe)H$_3$]·HFIP interaction, leading to short-

Table 2. Main energetic, structural, and charge parameters of the [CpW(dhpe)H$_3$]·TFE adducts. Energies are given relative to the separated reactants.

| | A | B | C | D |
|---|---|---|---|---|
| $\Delta E_{\text{gas phase}}$ [kcal mol$^{-1}$] | −9.7 | −11.9 | −11.0 | −8.5 |
| $\Delta E_{\text{BSSE}}$ [kcal mol$^{-1}$] | −5.0 | −8.4 | −6.4 | −4.1 |
| $\Delta E_{\text{DCM}}$ [kcal mol$^{-1}$] | −1.3 | −3.4 | −3.3 | −2.4 |
| dist. (O)H···H(W) [Å] | 1.742 | 2.126(H1)<br>1.771(H2) | 2.273 | 1.673 |
| dist. (O)H···W [Å] | 3.040 | 2.882 | 2.816 | 2.925 |
| ∢ O-H···H(W) | 151.5 | 139.8(H1)<br>161.8(H2) | 138.1 | 157.6 |
| ∢ O-H···W | 152.9 | 159.6 | 173.8 | 162.5 |
| $r_{\text{W–H1}}$ [Å][a] | 1.693 (−0.003) | 1.704 (0.008) | 1.696 (0.000) | 1.740 (0.044) |
| $r_{\text{W–H2}}$ [Å][a] | 1.733 (0.007) | 1.718 (−0.008) | 1.738 (0.012) | 1.725 (−0.001) |
| $r_{\text{W–H3}}$ [Å][a] | 1.742 (0.005) | 1.737 (0.000) | 1.739 (0.002) | 1.725 (−0.012) |
| $\Delta q_{\text{W}}$[b] | −0.005 | −0.106 | −0.163 | 0.016 |
| $\Delta q_{\text{H1}}$[b] | 0.002 | −0.015 | 0.015 | 0.007 |
| $\Delta q_{\text{H2}}$[b] | 0.003 | −0.041 | 0.011 | −0.040 |
| $\Delta q_{\text{H3}}$[b] | −0.064 | 0.011 | 0.003 | −0.036 |

[a] Value of $\Delta r$ ($r_{\text{compl}} - r_{\text{free}}$) in parentheses. [b] $\Delta q = q_{\text{compl.}} - q_{\text{free}}$.

Table 3. Main energetic, structural, and charge parameters of the [CpW(dhpe)$H_3$]·HFIP adducts. Energies are given relative to the separated reactants.

| | **A′** | **B1′** | **B2′** | **C1′** | **C2′** | **D′** |
|---|---|---|---|---|---|---|
| $\Delta E_{\text{gas phase}}$ [kcal mol$^{-1}$] | −10.4 | −12.8 | −12.6 | −12.3 | −10.9 | −9.6 |
| $\Delta E_{\text{BSSE}}$ [kcal mol$^{-1}$] | −4.9 | −8.6 | −8.1 | −6.6 | −5.3 | −3.5 |
| $\Delta E_{\text{DCM}}$ [kcal mol$^{-1}$] | 0.4 | −3.0 | −2.5 | −1.7 | −1.9 | −0.6 |
| dist. (O)H···H(W) [Å] | 1.706 | 1.812(H1)<br>1.919(H2) | 2.066(H1)<br>1.688(H2) | 2.032 | 1.809 | 1.725 |
| dist. (O)H···W [Å] | 3.020 | 2.792 | 2.822 | 2.690 | 2.612 | 2.898 |
| ∢ O−H···HW | 151.7 | 154.0(H1)<br>140.8 (H2) | 139.2 (H1)<br>158.0(H2) | 133.0 | 142.1 | 151.5 |
| ∢ O−H···W | 150.6 | 166.9 | 164.2 | 172.8 | 176.7 | 158.9 |
| $r_{\text{W–H1}}$ [Å][a] | 1.694 (−0.002) | 1.706 (0.010) | 1.715 (0.019) | 1.696 (0.000) | 1.723 (0.027) | 1.739 (0.043) |
| $r_{\text{W–H2}}$ [Å][a] | 1.734 (0.008) | 1.718 (−0.008) | 1.708 (−0.018) | 1.734 (0.008) | 1.734 (0.008) | 1.723 (−0.003) |
| $r_{\text{W–H3}}$ [Å][a] | 1.743 (0.006) | 1.736 (−0.001) | 1.737 (0.000) | 1.739 (0.002) | 1.728 (−0.009) | 1.724 (−0.013) |
| $\Delta q_{\text{W}}$[b] | −0.005 | −0.130 | -0.102 | −0.189 | −0.149 | 0.024 |
| $\Delta q_{\text{H1}}$[b] | 0.003 | −0.014 | −0.039 | 0.016 | −0.002 | 0.012 |
| $\Delta q_{\text{H2}}$[b] | 0.006 | −0.067 | −0.065 | 0.012 | 0.003 | −0.038 |
| $\Delta q_{\text{H3}}$[b] | −0.084 | 0.016 | 0.014 | −0.018 | −0.037 | −0.067 |

[a] Value of $\Delta r$ ($r_{\text{compl}}-r_{\text{free}}$) in parentheses. [b] $\Delta q = q_{\text{compl}}-q_{\text{free}}$ [c] Calculated intensity in parentheses ($A$, $10^4$ L mol$^{-1}$ cm$^{-2}$).

er (W)H···H(O) and W···H(O) distances in structures **A″**–**D″** and to nearly linear W···H−O angles in structures **B″**–**D″**, illustrating the effect of cooperativity in hydrogen bonding.

The most stable adducts are **B** for TFE (−11.9 kcal mol$^{-1}$ relative to the separated species) and **B1′** for HFIP (−12.8 kcal mol$^{-1}$), involving the main interaction with a hydride ligand and the metal. However, the isomers involving the main interaction with the metal atom (**C** for TFE and **C1′** for HFIP) are only marginally less stable, whereas the adducts in which the proton donor interacts mostly with the H3 site (**A/A′** and **D/D′**) are significantly less stable, in spite of the fact that this hydride ligand appears the most hydridic in the trihydride ground-state structure (see Figure 2). Note that, for each pair of structurally related adducts, HFIP shows a stronger interaction than TFE by approximately 1 kcal mol$^{-1}$, in agreement with the stronger acidity of the former. In quantitative terms, the uncorrected gas-phase values are too high, the gas-phase BSSE-corrected values are closer, whereas the values calculated using the polarizable continuum model for the solvent are too small. The ordering of the two most stable species is preserved upon introducing the BSSE correction and the PCM.

The energy ordering found for the [CpW(dhpe)$H_3$]·TFE adducts parallels that previously observed for the corresponding [CpMo(dhpe)$H_3$]·TFE adducts.[29] For each pair of structurally related adducts, the W complex shows a stronger interaction than the Mo analogue, in agreement with the stronger basicity of the former. The preference for **B** versus **C** is nearly the same for the two metal systems. However, it is interesting to note that the relative contribution of the metal atom to the H-bonding interaction increases on going from Mo to W in both adducts **B** and **C** (Figure 7). For both species, the H···H distance only marginally shortens (for H2 in **B**) or lengthens (for H1 in **B** and for H3 in **C**), whereas significant shortening would be expected for dihydrogen bonding to a stronger base. At the same time, the M···H distance becomes significantly shorter on going from Mo to W. In conclusion, the calculations suggest that the preferred H-bonded species for the [CpM(dhpe)$H_3$] (M = Mo, W) model complexes feature bifurcate interactions with both M and H, rather than with either a metal lone pair or hydride ligand solely. However, the metal-atom contribution increases on going from Mo to W.

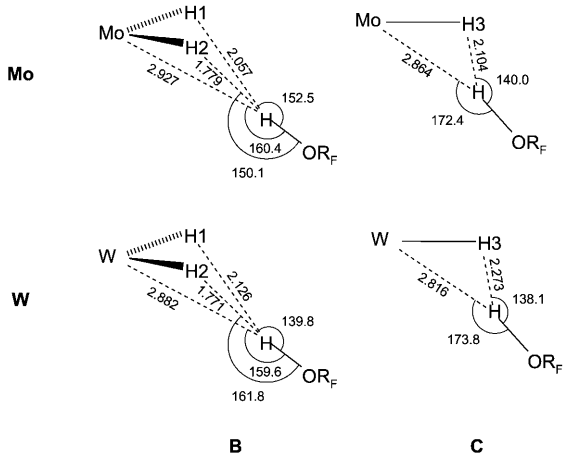


Figure 7. Comparison of H-bond lengths and angles for the [CpM(dhpe)$H_3$]·TFE adducts **B** and **C** (M = Mo, W).

The only previous theoretical work addressing the metal influence on hydrogen bonding is the study of dihydrogen-bonded complexes of [$MH(CO)_2(NO)(PH_3)_2$] (M = Mo, W) with HF by Orlova and Scheiner.[49] Their B3PW91 computations revealed the dihydrogen-bonded complex of tungsten hydride to be only 0.3 kcal mol$^{-1}$ more stable than that of molybdenum. The presence of strong π-accepting ligands, CO and NO, makes the metal atom in these hydride complexes a poor proton acceptor. Thus, the relatively short M···H(F) contact found is only an additional interaction, which, in contrast to the trihydrides discussed herein, lengthens on going from MoH···HF to WH···HF.

**The proton-transfer product, [Cp*W(dppe)$H_4$]$^+$**: The quantitative protonation of complex [Cp*W(dppe)$H_3$] by $HPF_6$

  

and the X-ray structure of the resulting product, $[Cp^*W(dppe)H_4]PF_6$, have been described previously.[31] The product adopts a classical tetrahydride structure. In the present study, we investigated the proton-transfer processes using fluorinated alcohols of different strength and *p*-nitrophenol, as well as the strong acid $HBF_4$. NMR investigations carried out at low temperature reveal that in all cases the tetrahydride product is formed directly, without the detection of any intermediate (notably nonclassical species). This behavior is identical to that of the Mo analogue.[29] Before discussing the details of the interaction with the weaker acids, we analyze in more detail the nature of the proton-transfer product from the experimental and computational points of view.

The optimized geometry of the model $[CpW(dhpe)H_4]^+$ complex (Figure 8) is in agreement with the X-ray data presented earlier for $[Cp^*W(dppe)H_4]^+PF_6^-$.[31] An even closer

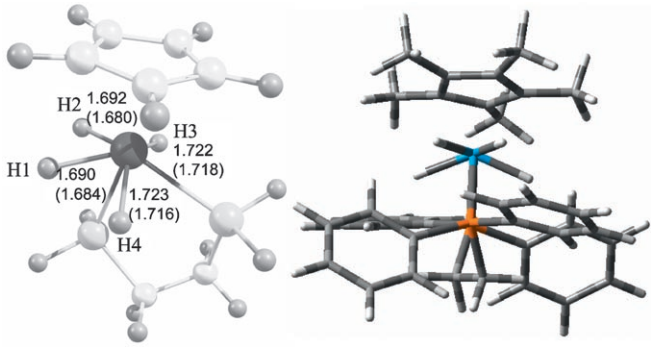


Figure 8. Left: Optimized geometry of the $[CpWH_4(dhpe)]^+$. W–H bond lengths are in Å. The values in parentheses correspond to those optimized for the real cation (right).

agreement is obtained by optimization of the system with the real ligands (Figure 8). This geometry is also very close to that optimized for the analogous Mo complex.[29] A second, higher-energy isomer was also located (see Supporting Information). On the other hand, at variance with the Mo analogue, no stable minimum could be located for a nonclassical isomer, namely a dihydrogen complex of type $[CpW(dhpe)(\eta^2\text{-}H_2)H_2]^+$. This is in line with the preference of (early) third-row transition-metal polyhydrides to exist as classical species.[50,51]

The coordination geometry of the energy minimum can be viewed as a distorted pentagonal bipyramid, with four hydride ligands and one of the phosphorus atoms describing the pentagonal plane and the second phosphorus atom and the Cp* ring centroid in the axial positions. The hydride ligands bear similar small positive Mulliken charges of approximately 0.06 units, but differ in distance to the metal (Figure 8). Correspondingly, the frequency calculations give two pairs of normal modes that can be described as symmetric and asymmetric stretching vibrations involving pairs of equivalent hydrides (Figure 9). This is in good agreement with the experimentally observed spectrum of $[Cp^*W(dppe)H_4]^+BF_4^-$, which features two lower- and two higher-intensity bands after the subtraction of dppe overtones (see Figure S3 in the Supporting Information).

The proton affinity of the tungsten trihydride, calculated as $-\Delta H$ (298 K) for the reaction with $H^+$, is 255.1 kcal mol$^{-1}$ with respect to more stable $[CpWH_4(dhpe)]^+$ isomer, being only 15 kcal mol$^{-1}$ higher than that for the analogues molybdenum complex (240.3 kcal mol$^{-1}$). When taking into account the real system, the proton affinities of the metal hydrides increase by about 20 kcal mol$^{-1}$ for both the tungsten and the molybdenum complexes, being 274.5 and 263.2 kcal mol$^{-1}$, respectively.

**Experimental study of the proton-transfer thermodynamics**: As mentioned above, the interaction of $[Cp^*W(dppe)H_3]$ with fluorinated alcohols results in partial protonation, the extent of which depends on the strength and amount of proton donation. The proton-transfer equilibrium for the $[Cp^*W(dppe)H_3]$/HFIP system was investigated in toluene by UV spectroscopy in the 190–240 K range. The trihydride complex shows a wide band at 425 nm ($\Delta\lambda_{1/2} = 100$ nm) with an extinction coefficient of 2128 M$^{-1}$ cm$^{-1}$, whereas the tetrahydride complex has a negligible absorption in this region (Figure 10). The UV-visible properties of the hydrogen-bonded complexes are essentially indistinguishable from those of the free hydride complex.[24,29] Upon addition of three equivalents of HFIP at 190 K, 90% of the complex converts to the tetrahydride product, leading to a decrease in absorption intensity. This intensity slowly increases upon heating, demonstrating the reversibility of the proton-transfer process, the equilibrium shifting toward the trihydride complex as the temperature increases. These spectral

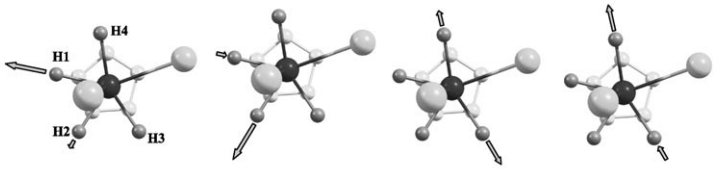


| | $\nu_1$ = 1975 cm$^{-1}$ | $\nu_2$ = 1960 cm$^{-1}$ | $\nu_3$ = 1892 cm$^{-1}$ | $\nu_4$ = 1860 cm$^{-1}$ |
|---|---|---|---|---|
| *A* | 0.112 | 0.098 | 0.316 | 0.314 |
| W-H1 | ***0.969*** | 0.015 | 0.010 | 0.005 |
| W-H2 | 0.015 | ***0.970*** | 0.003 | 0.011 |
| W-H3 | 0.014 | 0.001 | ***0.602*** | ***0.379*** |
| W-H4 | 0.000 | 0.013 | ***0.384*** | ***0.600*** |

Figure 9. W–H normal modes of the DFT optimized $[CpWH_4(dhpe)]^+$ with their frequency, intensity (*A*, $10^4$ L mol$^{-1}$ cm$^{-2}$), and potential-energy distribution (major components are in bold italic). The Cp- and P-bonded H atoms and ethylene backbone have been omitted for clarity.

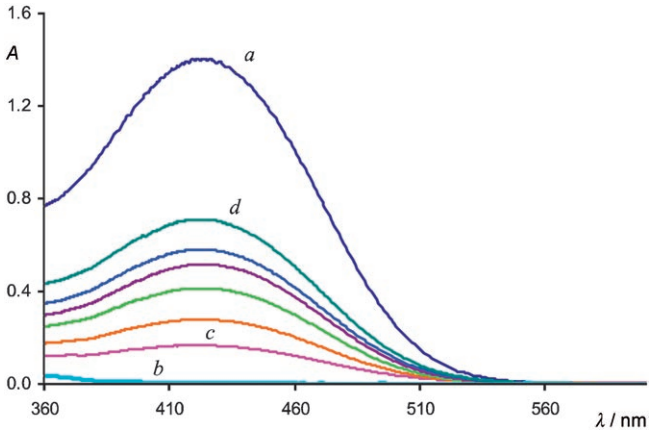


Figure 10. UV/Vis spectra of $[Cp^*W(dppe)H_3]$ (0.0015 M in toluene, 0.22-cm cell): a) alone; b) $[Cp^*W(dppe)H_4]^+[OCH(CF_3)_2]^-$ obtained by addition of 30 equiv HFIP, and c–d) in the presence of HFIP (0.0045 M) over 10-K temperature increments in the 190–240 K range.

changes allowed calculation of the proton-transfer equilibrium constants [Eq. (2)], assuming that the ionic complex has the same 1:1 composition as determined for *p*-nitrophenol (see below).

$$[WH_3] + R^FOH = [WH_3]\cdots HOR^F = [WH_4]^+\cdots OR^{F-} \quad (2)$$
$$K_1 \qquad\qquad K_2$$

Taking into account the $K_1$ constants determined by IR spectroscopy for the hydrogen-bond formation (see above), the van't Hoff analysis yielded the proton-transfer-equilibrium constant in toluene, $K_2$, at each temperature and consequently $\Delta H_2 = -3.9 \pm 0.3$ kcal mol$^{-1}$ and accordingly $\Delta S_2 = -17 \pm 2$ cal mol$^{-1}$ K$^{-1}$. Unfortunately, no direct comparison can be made to thermodynamics of hydrogen bonding and proton transfer of other systems ($[Cp^*FeH(dppe)]$ + HFIP,[25] or $[Cp^*MoH_3(dppe)]$ + TFE[29]) because the latter were obtained in a more polar solvent, $CH_2Cl_2$. However, considering that the less polar toluene solvent should disfavor proton transfer, the present system, $[Cp^*WH_3(dppe)]$ + HFIP, gives the highest proton-transfer-enthalpy value, in agreement with the greater basicity of the trihydride complex.

The $[Cp^*W(dppe)H_3]$ protonation was also investigated by using *p*-nitrophenol (PNP). This proton donor has the advantage of being a convenient chromophore, with an absorption band centered at quite different positions in the visible region as a function of protonation state (neutral phenol, H-bonded phenol, H-bonded or free anion). The exact band positions and extinction coefficients are solvent and temperature dependent: for example, PNP absorbs at 309–318 nm ($\log\varepsilon = 9.36$–$9.57$) in THF, at 305–312 nm ($\log\varepsilon = 8.99$–$9.21$) in $CH_2Cl_2$,[25] and at 300–310 nm ($\log\varepsilon = 7.50$–$7.67$) in toluene in the 290–200 K range. The *p*-nitrophenolate anion (as $Bu_4N^+$ salt) shows a band at 430–425 nm ($\log\varepsilon = 10.22$–$10.24$) in THF, and at 433–428 nm ($\log\varepsilon = 10.21$–$10.22$) in $CH_2Cl_2$ in the same range.

As was previously observed for other hydrides interacting with *p*-nitrophenol ($[Cp^*FeH(dppe)]$,[25] $[Cp^*MoH_3(dppe)]$,[29] and $[PP_3MH_2]$[33] with $PP_3 = P(CH_2CH_2PPh_2)_3$ and M = Fe, Ru, and Os), the UV/Vis spectra of PNP/$[Cp^*WH_3(dppe)]$ mixtures at 200 K in toluene exhibit a wide band of a complex shape, resulting from the overlap of three bands of PNP in its different forms: free phenol (310 nm), hydrogen-bonded phenol (339 nm), phenolate (376 nm), as well as the broad band of the trihydride complex at 425 nm. The phenolate band is blue-shifted from the free *p*-nitrophenolate band by 36 nm, because of hydrogen bonding to $[Cp^*WH_4(dppe)]^+$. A titration experiment (Figure 11) allowed establishment of the 1:1 stoichiometry of hydrogen-bonded ion pair $[Cp^*(dppe)WH_4]^+\cdots[OAr]^-$.

Note that an analogous study of complex $[Cp^*Fe(dppe)H]$ showed instead a 1:2 bonding stoichiometry, suggesting formation of a hydrogen-bonded ion pair between the non-classical cation and the homoconjugated anion $[Cp^*Fe(\eta^2\text{-}H_2)(dppe)]^+\cdots[ArOHOAr]^-$,[25] whereas the molybdenum analogue $[Cp^*Mo(dppe)H_3]$ shows again formation of a 1:1 ion pair with the *p*-nitrophenolate, $[Cp^*(dppe)MoH_4]^+\cdots[OAr]^-$.[29]

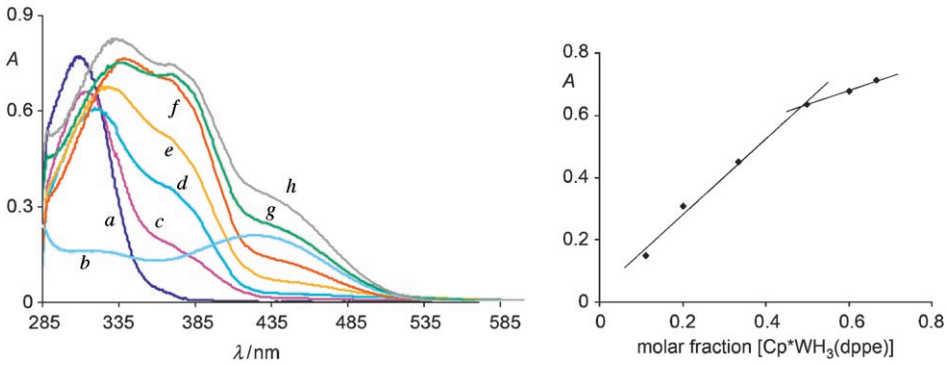


Figure 11. Left: UV/Vis spectra (toluene solution, 200 K, 0.12-cm cell) of: a) *p*-nitrophenol ($3\times10^{-4}$ M); b) $[Cp^*W(dppe)H_3]$ ($3\times10^{-4}$ M); c–h) *p*-nitrophenol in the presence of increasing amounts of $[Cp^*W(dppe)H_3]$: $3.7\times10^{-5}$ M (c), $7.5\times10^{-5}$ (d), $1.5\times10^{-4}$ (e), $3\times10^{-4}$ (f), $4.5\times10^{-4}$ (g), $6\times10^{-4}$ (h). Right: intensity changes at 380 nm.

The interesting solvent effect was noted for this system when THF was used. The equilibrium between PNP and $[Cp^*WH_3(dppe)]$ or PNP-anion and $[Cp^*WH_4(dppe)]BF_4$ (at 1:1 ratios) appeared to be completely shifted to the left in this solvent (envelop of the overlapping bands of "free" PNP and $[Cp^*WH_3(dppe)]$ were observed in both cases),

  

probably due to highly favored specific solvation of the phenol (hydrogen-bonding PNP·THF).

**Kinetics of the proton-transfer process**: The kinetics of $[Cp^*W(dppe)H_3]$ protonation was investigated by stopped-flow with UV/Vis detection in $CH_2Cl_2$ and toluene. The kinetics were studied at variable $WH_3/HOR^F$ ratios under pseudo-first-order conditions (large alcohol excess). The reaction with TFE, HFIP, and PFTB was explored, however, only the data obtained for PFTB lead to reliable results. The representative plots are shown in Figure 12. Surprisingly, a nonlinear dependence on the $HOR^F$ concentration was found for the observed rate constant, $k_{obs}$, in contrast to our previous kinetics studies on $[Cp^*Fe(dppe)H]$.[24]

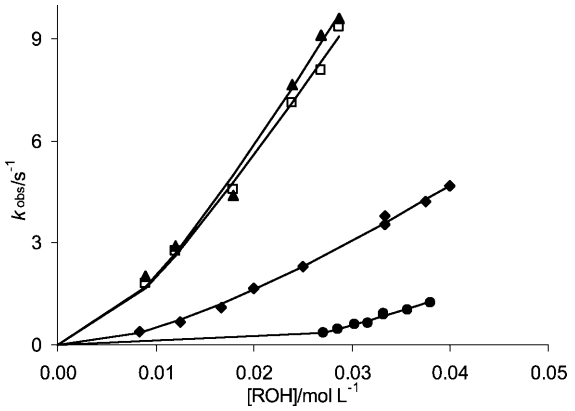


Figure 12. Dependence of the observed rate constant for the $[Cp^*W(dppe)H_3]$ protonation on the ROH concentration. ROH = HFIP in toluene at 293 K (●), PFTB in toluene at 293 K (◆), $CH_2Cl_2$ at 288 K (▲), and $CH_2Cl_2$ at 283 K (□). The solid lines correspond to the fitting according to Equation (4) (see text).

A straightforward rationalization of this behavior is possible on the basis of the previously established kinetic model, shown in Scheme 2. The resulting expression for the observed rate constant is represented in Equation (3):

$$k_{obs} = \frac{K_1 K_2 k[R^FOH]^2}{1 + K_1[R^FOH] + K_1K_2[R^FOH]^2} \quad (3)$$

The last term (proportional to the 1:2 adduct) can reasonably be neglected to yield Equation (4). According to this model, the $[R^FOH]$ dependence is a function of the hydrogen-bonding equilibrium: under conditions in which the dominant species is free hydride, the expression simplifies to

$$[Cp^*WH_3(dppe)] + R^FOH \underset{}{\overset{K_1}{\rightleftharpoons}} [Cp^*WH_3(dppe)]\cdots HOR^F$$

$$[Cp^*WH_3(dppe)]\cdots HOR^F + R^FOH \overset{K_2}{\rightleftharpoons} [Cp^*WH_3(dppe)]\cdots HOR^F\cdots HOR^F$$

$$[Cp^*WH_3(dppe)]\cdots HOR^F\cdots HOR^F \xrightarrow{k} [Cp^*WH_4(dppe)]^+ + [R^FOHOR^F]^-$$

Scheme 2. Kinetic model for proton transfer to $[Cp^*WH_3(dppe)]$.

yield a second-order dependence on $[R^FOH]$, whereas a first-order behavior is expected if the dominant species is the 1:1 adduct, $[Cp^*W(dppe)H_3]\cdots HOR^F$. The observed behavior is consistent with Equation (4):

$$k_{obs} \sim \frac{K_1 K_2 k[R^FOH]^2}{1 + K_1[R^FOH]} \quad (4)$$

in which the two terms in the denominator (proportional to free hydride and 1:1 adduct) are equally important, which allows a reasonable fit of the kinetics data, as shown in Figure 12.

The two independent parameters adjusted by the least-squares fitting are $K_1$ (in $L\,mol^{-1}$) and $(K_2k)$ (in $s^{-1}\,L\,mol^{-1}$), which are given in Table 4. The $K_2k$ parameter can be treated as an effective rate constant because the individual values of $K_2$ and $k$ are highly dependent on each other, making it impossible to derive them on the basis of these data. The values resulting from the data fitting for HFIP carry large uncertainties; no reasonable values could be obtained for the reaction with this alcohol in $CH_2Cl_2$. However, we include herein the data in toluene to discuss them at the qualitative level.

Table 4. Hydrogen-bond formation and proton-transfer rate constants for the reaction of $[Cp^*W(dppe)H_3]$ with alcohols.

| $R^FOH$ | solvent | $T$ [K] | $K_1$ [$L\,mol^{-1}$] | $K_2k$ [$s^{-1}\,L\,mol^{-1}$] | $\Delta G^{\neq}$ [$kcal\,mol^{-1}$] |
|---|---|---|---|---|---|
| HFIP | toluene | 293 | 13 | 165 | 14.2 |
| PFTB | toluene | 293 | 31 | 214 | 14.0 |
| PFTB | $CH_2Cl_2$ | 288 | 62 | 528 | 13.3 |
| PFTB | $CH_2Cl_2$ | 283 | 75 | 463 | 13.1 |

The values of hydrogen-bond formation constants, $K_1$, are in agreement with those estimated using H-bond enthalpy and entropy values obtained from IR data. Their increase on going from HFIP to PFTB is consistent with the greater proton-donor ability in H-bonding of PFTB. The $K_1$ values also increase on going from toluene to dichloromethane, as one could expect based on the ability of toluene to bind proton donors and, therefore, to lower their activity in hydrogen bonding.[45,52] The effective rate constants, $K_2k$, are higher for PFTB than for HFIP, in agreement with the stronger acidity of the former. The reaction rate substantially increases in more polar dichloromethane, the $K_2k$ values being more than double those in toluene, even at slightly lower temperatures.

It is also interesting to compare the above results with those obtained in the corresponding proton transfer by HFIP and PFTB to $[Cp^*Fe(dppe)H]$.[24] For the Fe system, more marked first-order behavior was observed for both proton donors. This is probably not related to greater $K_1$ values, because the iron hydride complex is a weaker base ($E_j = 1.36 \pm 0.02$) than the tungsten trihydride complex. Rather, it is related to the greater $[R^FOH]$ used in that study (in the 0.05–0.2 M range). The effective rate constants,

  

$K_2k$, are higher for [Cp*W(dppe)$H_3$] than for [Cp*Fe(dppe)H], in agreement with higher basicity of the tungsten complex and stronger interaction at the first reaction step, hydrogen bonding. The other notable difference between the two systems is that for the iron compound, $K_2k$ changes by more than one order of magnitude on going from PFTB to HFIP in $CH_2Cl_2$ (156 and 5.4 $s^{-1}$ L $mol^{-1}$, respectively), whereas the values are more similar for the tungsten trihydride complex and are markedly higher at that. This difference could be due to a smaller discrimination of the proton-donor strength in the case of the more basic W compound.

Table 5. Calculated proton-transfer reaction energies [kcal $mol^{-1}$].

| | Ion-pairing energy, $\Delta E_{IP}$[a] | | Proton-transfer energy, $\Delta E_{PT}$[b] | | Proton-transfer energy, $\Delta E'_{PT}$ | |
|---|---|---|---|---|---|---|
| | ion pair | in $CH_2Cl_2$ | separated ions | in $CH_2Cl_2$ | ion pair | in $CH_2Cl_2$ |
| [$CpWH_3$(dhpe)] | | | | | | |
| TFE | | | 118.9 | 36.2 | | |
| $(TFE)_2$ | | | 88.7 | 22.9 | | |
| HFIP | −95.7 | −15.1 | 98.0 | 22.0 | 13.3 (2.3)[c] | 8.7 (6.9) |
| $(HFIP)_2$ | −74.0 | −7.0 | 61.0 | 1.3 | 1.7 (−13.0)[d] | −3.1 (−5.7) |
| [Cp*$WH_3$(dppe)] | | | 99.2 | 28.6 | | |
| $(TFE)_2$ | | | 69.1 | 10.4 | | |
| HFIP | −81.8 | −13.5 | 78.4 | 14.3 | 8.7 (−3.4)[e] | 4.7 (0.8) |
| $(HFIP)_2$ | −65.0 | −8.4 | 41.4 | −11.5 | −7.4 (−23.6)[e] | −11.4 (−19.9) |

[a] Relative to the separated ions. [b] Relative to the separated neutral reactants. [c] Ion pair relative to the H-bonded adduct **C2′** presented in the reaction coordinates (Figure 13) and, in parentheses, to the separated neutral reactants. [d] Ion pair relative to the H-bonded adduct **D″** presented in the reaction coordinates (Figure 14) and, in parentheses, to the separated neutral reactants. [e] For structures, see Figure S5 in Supporting Information.

The values of $k_{obs}$ do not greatly change in response to temperature (Figure 12). This is probably due the to simultaneous dependence of $K_1$, $K_2$, and $k$ on temperature: whilst the two equilibrium constants are expected to decrease as temperature increases (the H-bond formation is exothermic), the proton-transfer rate constant increases. Thus, two effects cancel each other out. The activation free energy, $\Delta G^{\neq}$, values calculated from the rate constants in Table 4 are notably lower than those for the above-mentioned [Cp*Fe(dppe)H] system in $CH_2Cl_2$ ($\Delta G^{\neq}_{298\,K} = 14.5$ kcal $mol^{-1}$ for PFTB and 16.5 kcal $mol^{-1}$ for HFIP).

**Computational study of the proton-transfer process**: To estimate the energy barrier and the energy gain associated with the proton-transfer process, the reaction coordinate leading from the hydrogen-bonded species to the tetrahydride product was studied both in the gas phase and in $CH_2Cl_2$ by computational methods. The calculations explain how several factors, namely ion pairing, alcohol strength, substituent (Me, Ph), and solvent effects, contribute to the product stabilization, resulting in the net exothermic proton-transfer process observed for the real system.

As mentioned above, [$CpWH_3$(dhpe)] possesses quite high proton affinity (energy of the reaction with $H^+$ is highly negative). However, when two neutral species (the trihydride and the alcohol) are converted to two isolated charged species in the gas phase, the proton-transfer products are highly destabilized because of the charge separation (Table 5). This energy penalty, $\Delta E_{PT}$, is lowered upon considering the effect of a second alcohol molecule, which affords a hydrogen-bonded $(ROH)_2$ species on the side of the reactants and a homoconjugate anion, $(RO\cdots H\cdots OR)^-$ on the side of the product. As the presence of the methyl substituents on the Cp ring and the phenyl one on the P-ligands allows a better stabilization of the positive charge, these energies appeared to be substantially lower for the real system. As may be expected, the acidic strength of the proton donor also affects considerably the thermodynamics of the proton transfer, making it more favorable on going from TFE to HFIP. Finally, the solvent plays a major role in stabilizing the charged species: calculations with the polarizable continuum model (PCM) in $CH_2Cl_2$ show the markedly reduced endothermicity. As a result, for the reaction of [Cp*$WH_3$(dppe)] with two HFIP molecules in $CH_2Cl_2$, the separated ions are found 11.5 kcal $mol^{-1}$ below the neutral reactants.

Until now we have considered separated anion and cation as the product, however, ion-pair formation between the tetrahydride cation and the anion may be expected in $CH_2Cl_2$ solution. Thus, ion pairs with one and two HFIP units were optimized for the model and real cations (for the latter structures, see Figure S5 in Supporting Information). Formation of a hydrogen-bonded ion pair with HFIP anions is highly favorable not only in the gas phase, but also in solution (Table 5). Note that the ion-pairing energy, $\Delta E_{IP}$, is lower for the homoconjugate anion, $[(CF_3)_2CHO\cdots H\cdots OCH(CF_3)_2]^-$, in agreement with its lower basicity relative to simple $[(CF_3)_2CHO]^-$. This can also be appreciated from the (W)H···O distances (with one HFIP the H···O distance is 2.460 Å, and with two, the distance from the two oxygen atoms are 3.143 and 3.166 Å) As the result of the ion-pairing stabilization, the proton-transfer reaction energy, $\Delta E'_{PT}$, becomes less endothermic and even exothermic and remains such in solution. Notably, despite the destabilization of all the species, passing from the gas phase to solution makes the proton-transfer reaction more favorable.

To estimate the energy barrier associated with the proton-transfer process, the reaction coordinate leading from the hydrogen-bonded species to the tetrahydride product was studied both in the gas phase and in $CH_2Cl_2$ by computational methods. The proton-transfer process from HFIP to the model complex, [$CpWH_3$(dhpe)], was the subject of a more complete investigation along the proton-transfer pathway, using the O–H distance of the HFIP molecule as the key parameter. Species **C2′**, featuring interaction with the W and H3 atoms, was chosen for the proton-transfer-coordinate study by analogy to the previous Mo study.[29] The re-

  

sults obtained in the gas phase and in dichloromethane are presented in Figure 13. The coordinate presents a maximum at 18.7 kcal mol$^{-1}$ in the gas phase, and 14.9 kcal mol$^{-1}$ in $CH_2Cl_2$, for an O–H distance of 1.7 Å. The W–H distance is 1.786 Å and the distance between the transferring proton and the closest hydride is 1.855 Å. Thus, there is no indication for the formation of a nonclassical $H_2$ complex along this proton-transfer pathway.

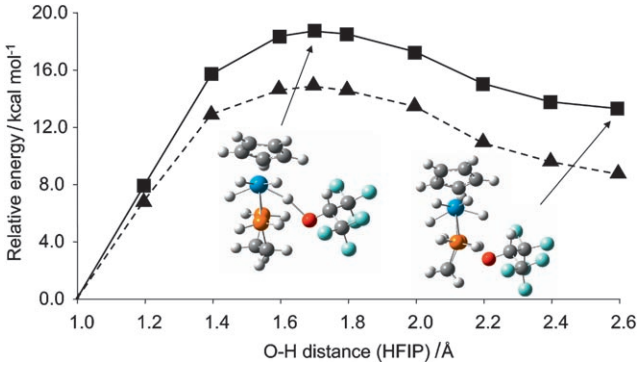


Figure 13. Proton-transfer reaction coordinates for species **C2′** in the gas phase and in dichloromethane. Solid line and squares: in the gas phase; dashed line and triangles: in dichloromethane solution. The O–H length of the transferring proton was taken as the reaction coordinate.

The minimum located at the end of the reaction coordinate presents a geometry close to that of the isolated tetrahydride complex, the W–H distances being 1.695, 1.693, 1.693, and 1.724 Å (cf. 1.690, 1.692, 1.722, and 1.723 for the isolated tetrahydride complex). The deprotonated base of the proton donor is still in proximity and interacts with the ligands. Instead of the expected (W)H···O($R_F$) bond, the oxygen atom is located near a phosphine group, (P)H···O($R_F$) = 2.457 Å, and the newly formed W–H bond is in close proximity to one of the anion C–H bonds, (W)H···H(C) = 2.084 Å. This result is clearly related to the use of the dhpe model. The barriers calculated for this process are sensibly lower than those for the same process occurring at the analogous Mo complex (24.7 and 22.8 kcal mol$^{-1}$ in the gas phase and in $CH_2Cl_2$, respectively).[29]

Because the proton-transfer reaction from fluorinated alcohols was shown to involve the active participation of a second proton-donor molecule (see above), we also investigated the reaction coordinates considering two HFIP molecules. Two [CpW(dhpe)$H_3$]·2 HFIP minima (**C2″** and **D″**, see Supporting Information) were chosen for this study. Species **C2″** is configurationally related to that of above-described investigation with a single HFIP molecule, except that the interaction is stronger with W and weaker with H3, whereas **D″** exhibits a much stronger interaction with the H3 ligand and a weaker one with W. Both pathways yield an earlier maxima on the proton-transfer reaction coordinates and lower energy barriers than the pathway involving a single HFIP molecule, paralleling the results reported previously for the ([Cp*Fe(dppe)H] + 2 $CF_3COOH$) and ([Cp*Mo(dppe)$H_3$] + 2 HFIP) systems.[29] The lower-energy pathway is that resulting from adduct **D″**, the results being presented in Figure 14 (those obtained from **C2″** are presented in the

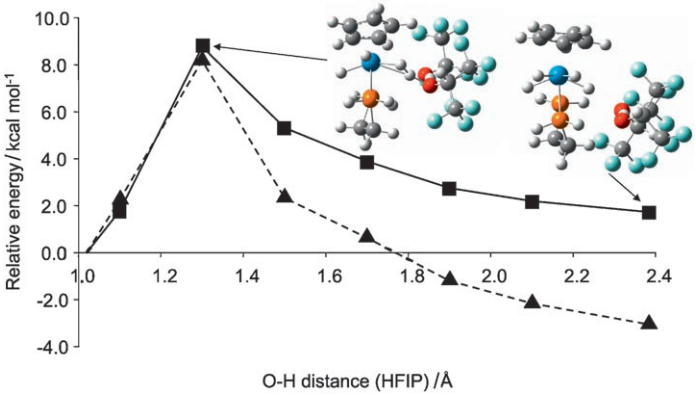


Figure 14. Proton-transfer reaction coordinate for species **D″** in the gas phase and in dichloromethane. Plain curve and squares: in the gas phase; dashed line and triangles: in dichloromethane solution. The O–H length of the transferring proton was taken as the reaction coordinate.

Supporting Information). The maximum of the potential-energy curve is located at 8.7 kcal mol$^{-1}$ in the gas phase and 8.8 kcal mol$^{-1}$ in dichloromethane, for an O–H distance of 1.3 Å (cf. 10.6 and 9.0 kcal mol$^{-1}$, respectively, for the **C2″** pathway). These barriers are lower than those calculated for the Mo system (11.2 and 9.4 kcal mol$^{-1}$ in the gas phase and in dichloromethane, respectively). The geometry of the maximum shows a small H–H distance of 1.102 Å and a W–H distance for the transferring proton of 2.215 Å. Thus, this structure may be described as an asymmetric, nonclassical species. However, no stable minimum corresponding to a nonclassical intermediate could be located along the proton-transfer pathway. The product of the proton transfer shows once again the geometry of the stable tetrahydride minimum, with W–H distances of 1.725, 1.698, 1.686, 1.710 Å, with weak interaction with the anionic group through the transferred hydride ligand, (W)H···O = 2.384 Å, and the phosphine H atom, (P)H···O = 2.083 Å.

## Discussion

The main interest of this work resides in the comparison of basicity, hydrogen bonding, and proton-transfer mechanism of the two homologous complexes [Cp*M(dppe)$H_3$] (M = Mo, W). The two compounds adopt an identical structure and are reversibly protonated to yield an identical classical tetrahydrido product, [Cp*M(dppe)$H_4$]$^+$, without detection of a nonclassical intermediate. However, whereas the Mo complex can loose $H_2$ in coordinating solvents or in the presence of coordinating anions,[30,31] the W complex is stable under the same conditions.[31] Thus, a reasonable question is whether the preferred position of hydrogen bonding and proton transfer may be the metal site and

  

whether the reaction mechanism may be different for two metal hydrides. For the Mo species, the experimental results[29] suggest that the hydrogen bonding occurs at a hydride ligand, and an additional interaction with the metal atom is revealed by calculations. However, this H-bonded intermediate leads to the final classical tetrahydride product without experimental detection of an intermediate dihydrogen complex, $[Cp^*Mo(dppe)(\eta^2\text{-}H_2)H_2]^+$. Calculations on the proton-transfer pathway for the model $[CpMo(dhpe)H_3]$ system revealed the existence of the dihydrogen complex $[CpMo(dhpe)(\eta^2\text{-}H_2)H_2]^+$ in a shallow local minimum, and the rearrangement to the classical tetrahydrido isomer occurs with an extremely small barrier.

The present $[Cp^*W(dppe)H_3]$ system displays a record high basicity in hydrogen bonding ($E_j = 1.74 \pm 0.03$ compared to the value of $1.42 \pm 0.02$ for the Mo analogue). Thus, one could expect similar but more pronounced spectroscopic changes if the hydrogen-bonding sites would be the same for two metal systems. But this is not the case; the different IR-spectroscopic results observed for the hydrogen bonding to two hydrides suggest differences in the structure of H-complexes. The DFT calculations of the hydrogen-bonded complexes reproduce the experimental finding of the stronger interactions in the order W > Mo and HFIP > TFE. The geometry optimization in the gas phase reveals also that for either metal system the preferred H-bonded structures feature interactions with both metal atom and hydride ligand, however, a M···HO contribution increases and a M–H···HO contribution decreases on going from Mo to W.

A second important difference is that no $[CpW(dhpe)(\eta^2\text{-}H_2)H_2]^+$ intermediate was located along the proton-transfer pathway by the DFT calculations, but one of the possible reaction-coordinate maxima (the lowest-energy one) has a nonclassical character. It may be stated that the protonation process involves a direct transfer to the metal site, although involving assistance by a hydride ligand. The absence of a nonclassical minimum is also suggested qualitatively by experimentally observed differences in reactivity. Whereas the Mo complex loses $H_2$ in coordinating solvents or in the presence of coordinating anions,[30,31] the W complex is stable under the same conditions.[31]

As hydrogen bonding can be regarded as the incipient stage of proton transfer, the protonation occurs easier, that is, the proton-transfer barrier becomes lower, as the base becomes stronger. Indeed, the proton-transfer barrier estimated from the stopped-flow kinetic data for $[Cp^*WH_3(dppe)]$ is lower than for $[Cp^*FeH(dppe)]$ with the same alcohols (HFIP or PFTB), in agreement with the greater basicity of the tungsten complex. This involves the active participation of the second alcohol molecule, which as shown by theoretical calculations for this and other systems,[24,25] strengthens the primary hydrogen bond through a cooperative effect and lowers the proton-transfer barrier. However, the 1:1 composition was determined for the proton-transfer product, the hydrogen-bonded ion pair $[Cp^*WH_4(dppe)]^+ \cdots [OR]^-$, whereas a 1:2 stoichiometry was found for the protonation of $[Cp^*MH(dppe)]$[25,27] and $PP_3MH_2$ hydrides,[33] yielding $[L_nM(\eta^2\text{-}H_2)]^+ \cdots [ROHOR]^-$. A possible rationalization of this phenomenon could be the weaker acidity of classical polyhydride species relative to nonclassical ones, so it can be stabilized by stronger interaction with $[OR]^-$ and withstand a deprotonation.[34] This rationalization finds support in the computational results.

According to both experimental and theoretical results the protonation reaction is more exothermic for the W system, in agreement with its greater basicity in hydrogen bonding and proton affinity. The thermodynamic parameters of hydrogen bonding and proton transfer were obtained for $[Cp^*WH_3(dppe)] + HFIP$ in toluene. Due to the solvent effect[45,52] these values are lower than they would be in $CH_2Cl_2$ (the solvent used for other studies, $[Cp^*FeH(dppe)] + HFIP$,[25] or $[Cp^*MoH_3(dppe)] + TFE$[29]). Nevertheless, they exceed other systems in agreement with the greater basicity of the tungsten trihydride complex.

The cumulative experimental and theoretical results allow different reaction energy profiles to be drawn for the Mo and W systems, as shown in Figure 15. The stronger H-bonding, greater stability of the tetrahydrido protonation product, and lower activation barrier for the proton-transfer step are the salient features of the tungsten system in respect to the molybdenum congener. The stronger participation of the metal in hydrogen bonding assists the direct proton transfer to the tungsten atom, and the dihydrogen complex found for molybdenum disappears as a minimum along the reaction pathway in the case of tungsten. Such differences in the proton-transfer mechanism and the character of the energy profile could be expected for hydride complexes of electron-rich metals bearing donor ligands descending the group (from 2nd to 3rd transition row).

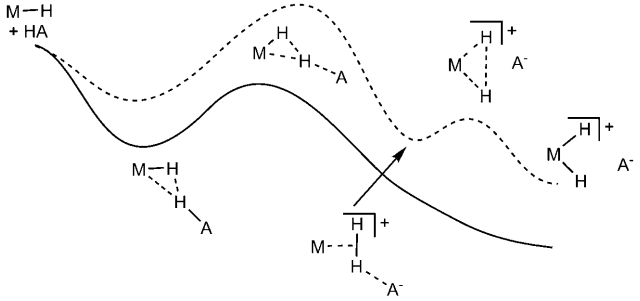


Figure 15. Qualitative energy profile for the proton transfer to $[Cp^*M(dppe)H_3]$ (M = Mo, dashed curve; W, solid curve).

## Conclusion

Basic knowledge accumulated over the last two decades suggests that a direct proton transfer to a metal lone pair is an unlikely event in the presence of hydride ligands, which are considered to be the kinetic site of the proton attack even if a classical di-(poly)hydride would be a thermodynamic protonation product. According to both experimental and theo-

  

retical results presented herein, the greater metal basicity for tungsten in [Cp*W(dppe)$H_3$] leads to stronger H-bonding, and to the more exothermic protonation reaction having a lower activation barrier, relative to the Mo analogue. In this work evidence was obtained for the first time for stronger (relative to the proton–hydride interaction) participation of the metal in hydrogen bonding affecting the subsequent proton-transfer profile, which involves a direct proton transfer to the metal center without the formation of a nonclassical intermediate.

## Experimental Section

**General**: All manipulations were performed under an argon atmosphere by using standard Schlenk techniques. All solvents were dried over appropriate drying agents (Na/benzophenone for toluene or THF, $CaH_2$ for $CH_2Cl_2$) and freshly distilled under an argon atmosphere prior to use. The NMR solvents (Aldrich) were degassed by three freeze–pump–thaw cycles, and then purified by vacuum transfer at room temperature. Compound [Cp*W(dppe)$H_3$] was synthesized according to literature.[31]

**Spectroscopic studies**

**NMR investigations**: Samples of the hydride [Cp*W(dppe)$H_3$] in [$D_8$]toluene were prepared under an argon atmosphere in 5-mm NMR tubes. The $^1$H and $^{31}$P{$^1$H} data were collected by using a Bruker AV500 spectrometer, operating at 500.3 and 202.5 MHz, respectively. The temperature was calibrated using a methanol chemical-shift thermometer; the accuracy and stability was $\pm 1$ K. All samples were allowed to equilibrate at every temperature for at least 3 min. The spectra were calibrated with the residual solvent resonance ($^1$H) and with external 85% $H_3PO_4$ ($^{31}$P). The conventional inversion-recovery method (180-$\tau$-90) was used to determine the variable-temperature longitudinal relaxation time $T_1$. Standard Bruker software was used for the calculation of the longitudinal relaxation time.

**IR and UV/Vis investigations**: The IR measurements were performed by using the "Infralum 801" FTIR spectrometer with $CaF_2$ cells of 0.04–0.22-cm path length. The UV measurements were performed by using Specord M-40 and Varian Cary 5 spectrophotometers. All measurements were carried out by use of a home-modified cryostat (Carl Zeiss, Jena) in the 190–290-K temperature range. The cryostat modification allows operation under an inert atmosphere and transfer of the reagents (premixed either at low or RT) directly into the cell pre-cooled to the required temperature. The accuracy of the temperature adjustment was $\pm 1$ K.

**Computational details**: Calculations were performed using the Gaussian 98[53] package at the DFT/B3LYP level.[54–56] Effective core potentials (ECP) were used to represent the innermost electrons of the tungsten atom as well as the electron core of phosphorous atoms.[57,58] The basis set for the W and P atoms was that associated with the pseudopotential,[57,58] with a standard double-$\zeta$ LANL2DZ contraction,[53] supplemented in the case of P with a set of d-polarization functions.[59] The carbon and hydrogen atoms of the transition-metal complexes that are not bonded to the metal atom, together with the atoms of proton-donor molecules (C, F, H) that are not involved in hydrogen bonds, were described with a 6–31G basis set.[60] The carbon and hydrogen atoms directly bonded to the metal and the proton-donor molecules (hydrogen and oxygen atoms) involved in hydrogen bonding were described with a 6–31G(d,p) set of basis functions.[61] Geometry optimizations were carried out without symmetry restrictions. Given the impossibility of locating the transition states in solution for technical reasons, the potential-energy curves were explored from reactants to products by series of partial optimizations in the gas phase. All the parameters were optimized except for the O–H distance that was increased by 0.2 Å at each step. The energy corresponding to each O–H distance was then evaluated in solution, and the maximum energy obtained along the resulting curve was taken to give the maximum point of the coordinate. Solvent effects were taken into account by means of polarized continuum model (PCM) calculations,[47,48] using standard options.[53] The solvation-free energies were computed in dichloromethane ($\varepsilon = 8.93$) at the gas-phase optimized geometries. The gas-phase complexation energies were corrected from the basis-set superposition error according to the counterpoise method of Boys and Bernardi.[46]

## Acknowledgements

We thank the European Commission through the HYDROCHEM program (contract HPRN-CT-2002–00176) for support of this work. Additional bilateral support (PICS, France–Russia; LEA LTPMM, France–Spain) and National support from the CNRS (France), from the Spanish MEC (Projects CTQ2005–09000-C02–01 and Consolider Ingenio 2010 CSD2007–00006), from the RFBR (05–03–22001, 08–03–00464), and the Division of Chemistry and Material Sciences of RAS (Russia), is also gratefully acknowledged. Dr. M. Baya thanks the Spanish Ministerio de Educación y Ciencia for a post-doctoral fellowship. The availability of the computational resources at the Centre de Supercomputació de Catalunya (CESCA) were also appreciated.

[1] G. W. Parshall, *Homogeneous Catalysis: The Applications and Chemistry of Catalysis by Soluble Transition-Metal Complexes*, Wiley, New York, **1980**, p. 230.
[2] A. Dedieu, *Transition-Metal Hydrides*, VCH, New York, **1992**.
[3] M. Peruzzini, R. Poli, *Recent Advances in Hydride Chemistry*, Elsevier, Amsterdam, **2001**.
[4] R. Y. Igarashi, M. Laryukhin, P. C. Dos Santos, H.-I. Lee, D. R. Dean, L. C. Seefeldt, B. M. Hoffman, *J. Am. Chem. Soc.* **2005**, *127*, 6231–6241.
[5] S. Foerster, M. Stein, M. Brecht, H. Ogata, Y. Higuchi, W. Lubitz, *J. Am. Chem. Soc.* **2003**, *125*, 83–93.
[6] R. Mejia-Rodriguez, D. S. Chong, J. H. Reibenspies, M. P. Soriaga, M. Y. Darensbourg, *J. Am. Chem. Soc.* **2004**, *126*, 12004–12014.
[7] N. V. Belkova, T. N. Gribanova, E. I. Gutsul, R. M. Minyaev, C. Bianchini, M. Peruzzini, F. Zanobini, E. S. Shubina, L. M. Epstein, *J. Mol. Struct.* **2007**, *844*, 115–131.
[8] L. M. Epstein, N. V. Belkova, E. I. Gutsul, E. S. Shubina, *Polish J. Chem.* **2003**, *77*, 1371–1383.
[9] N. V. Belkova, E. S. Shubina, L. M. Epstein, *Acc. Chem. Res.* **2005**, *38*, 624–631.
[10] R. H. Crabtree, *Encyclopedia of Supramolecular Chemistry*, **2004**, pp. 666–672.
[11] D. S. Trifan, R. Bacskai, *J. Am. Chem. Soc.* **1960**, *82*, 5010–5011.
[12] L. E. Vinogradova, A. Z. Kreindlin, L. A. Leites, I. T. Chizhevskii, E. S. Shubina, L. M. Epshtein, *Metalloorg. Khim.* **1990**, *3*, 1192.
[13] S. G. Kazarian, P. A. Hamley, M. Poliakoff, *J. Chem. Soc. Chem. Commun.* **1992**, 994–997.
[14] S. G. Kazarian, P. A. Hamley, M. Poliakoff, *J. Am. Chem. Soc.* **1993**, *115*, 9069–9079.
[15] P. A. Hamley, S. G. Kazarian, M. Poliakoff, *Organometallics* **1994**, *13*, 1767–1774.
[16] D. Braga, F. Grepioni, E. Tedesco, K. Biradha, G. R. Desiraju, *Organometallics* **1997**, *16*, 1846–1856.
[17] G. Parkin, J. E. Bercaw, *J. Chem. Soc. Chem. Commun.* **1989**, 255–257.
[18] M. S. Chinn, D. M. Heinekey, *J. Am. Chem. Soc.* **1990**, *112*, 5166–5175.
[19] G. Jia, A. J. Lough, R. H. Morris, *Organometallics* **1992**, *11*, 161–171.
[20] E. T. Papish, F. C. Rix, N. Spetseris, J. R. Norton, R. D. Williams, *J. Am. Chem. Soc.* **2000**, *122*, 12235–12242.
[21] J. R. Hamon, P. Hamon, L. Toupet, K. Costuas, J. Y. Saillard, *C. R. Chim.* **2002**, *5*, 89–98.
[22] C. Roger, P. Hamon, L. Toupet, H. Rabaâ, J.-Y. Saillard, J.-R. Hamon, C. Lapinte, *Organometallics* **1991**, *10*, 1045–1054.

  

[23] F. Maseras, A. Lledós, E. Clot, O. Eisenstein, *Chem. Rev.* **2000**, *100*, 601–636.
[24] N. V. Belkova, P. O. Revin, L. M. Epstein, E. V. Vorontsov, V. I. Bakhmutov, E. S. Shubina, E. Collange, R. Poli, *J. Am. Chem. Soc.* **2003**, *125*, 11106–11115.
[25] N. V. Belkova, E. Collange, P. Dub, L. M. Epstein, D. A. Lemenovskii, A. Lledós, O. Maresca, F. Maseras, R. Poli, P. O. Revin, E. S. Shubina, E. V. Vorontsov, *Chem. Eur. J.* **2005**, *11*, 873–888.
[26] M. Baya, O. Maresca, R. Poli, Y. Coppel, F. Maseras, A. Lledós, N. V. Belkova, P. A. Dub, L. M. Epstein, E. S. Shubina, *Inorg. Chem.* **2006**, *45*, 10248–10262.
[27] N. V. Belkova, P. A. Dub, M. Baya, J. Houghton, *Inorg. Chim. Acta* **2007**, *360*, 149–162.
[28] P. A. Dub, N. V. Belkova, K. A. Lyssenko, G. A. Silantyev, L. M. Epstein, E. S. Shubina, J.-C. Daran, R. Poli, *Organometallics* **2008**, *27*, 3307–3311.
[29] N. V. Belkova, P. O. Revin, M. Besora, M. Baya, L. M. Epstein, A. Lledós, R. Poli, E. S. Shubina, E. V. Vorontsov, *Eur. J. Inorg. Chem.* **2006**, 2192–2209.
[30] P. A. Dub, M. Baya, J. Houghton, N. V. Belkova, J. C. Daran, R. Poli, L. M. Epstein, E. S. Shubina, *Eur. J. Inorg. Chem.* **2007**, 2813–2826.
[31] B. Pleune, R. Poli, J. C. Fettinger, *Organometallics* **1997**, *16*, 1581–1594.
[32] E. Gutsul, N. Belkova, M. Sverdlov, L. Epstein, E. Shubina, V. Bakhmutov, T. Gribanova, R. Minyaev, C. Bianchini, M. Peruzzini, F. Zanobini, *Chem. Eur. J.* **2003**, *9*, 2219–2228.
[33] E. Gutsul, N. Belkova, G. Babakhina, L. Epstein, E. Shubina, C. Bianchini, M. Peruzzini, F. Zanobini, *Russ. Chem. Bull.* **2003**, *52*, 1204–1206.
[34] N. Belkova, M. Besora, L. Epstein, A. Lledós, F. Maseras, E. Shubina, *J. Am. Chem. Soc.* **2003**, *125*, 7715–7725.
[35] J. C. Fettinger, B. Pleune, R. Poli, *J. Am. Chem. Soc.* **1996**, *118*, 4906–4907.
[36] M. Baya, J. Houghton, J.-C. Daran, R. Poli, *Angew. Chem.* **2007**, *119*, 433–436; *Angew. Chem. Int. Ed.* **2007**, *46*, 429–432.
[37] M. Baya, J. Houghton, J.-C. Daran, R. Poli, L. Male, A. Albinati, M. Guttman, *Chem. Eur. J.* **2007**, *13*, 5347–5359.
[38] H. Sakaba, T. Hirata, C. Kabuto, K. Kabuto, *Organometallics* **2006**, *25*, 5145–5150.
[39] B. Pleune, D. Morales, R. Meunier-Prest, P. Richard, E. Collange, J. C. Fettinger, R. Poli, *J. Am. Chem. Soc.* **1999**, *121*, 2209–2225.
[40] L. M. Epstein, N. V. Belkova, E. S. Shubina in *Recent Advances in Hydride Chemistry* (Ed.: M. Peruzzini, R. Poli), Elsevier, Amsterdam, **2001**, pp. 391–418.
[41] A. V. Iogansen, *Theor. Experim. Khim.*, **1971**, *7*, 302–311.
[42] A. V. Iogansen, in *The Hydrogen Bond* (Ed.: N. D. Sokolov), Nauka, Moscow, **1981**.
[43] A. V. Iogansen, *Spectrochim. Acta Part A* **1999**, *55*, 1585–1612.
[44] E. Bakhmutova, V. Bakhmutov, N. Belkova, M. Besora, L. Epstein, A. Lledós, G. Nikonov, E. Shubina, J. Tomas, E. Vorontsov, *Chem. Eur. J.* **2004**, *10*, 661–671.
[45] A. Messmer, H. Jacobsen, H. Berke, *Chem. Eur. J.* **1999**, *5*, 3341–3349.
[46] S. F. Boys, F. Bernardi, *Mol. Phys.* **1970**, *19*, 553–566.
[47] J. Tomasi, M. Persico, *Chem. Rev.* **1994**, *94*, 2027–2094.
[48] C. Amovilli, V. Barone, R. Cammi, E. Cancès, M. Cossi, B. Menucci, C. S. Pomelli, J. Tomasi, *Adv. Quantum Chem.* **1998**, *32*, 227–261.
[49] G. Orlova, S. Scheiner, *J. Phys. Chem. A* **1998**, *102*, 260–269.
[50] Z. Lin, M. B. Hall, *J. Am. Chem. Soc.* **1992**, *114*, 6102–6108.
[51] Z. Lin, M. B. Hall, *Organometallics* **1993**, *12*, 4046–4050.
[52] A. V. Iogansen, *Theor. Experim. Khim.* **1971**, *7*, 312–317.
[53] M. J. Frisch, G. W. Trucks, H. B. Schlegel, G. E. Scuseria, M. A. Robb, J. R. Cheeseman, V. G. Zakrzewski, J. Montgomery, J. A., R. E. Stratmann, J. C. Burant, S. Dapprich, J. M. Millam, A. D. Daniels, K. N. Kudin, M. C. Strain, O. Farkas, J. Tomasi, V. Barone, M. Cossi, R. Cammi, B. Mennucci, C. Pomelli, C. Adamo, S. Clifford, J. Ochterski, G. A. Petersson, P. Y. Ayala, Q. Cui, K. Morokuma, D. K. Malick, A. D. Rabuck, K. Raghavachari, J. B. Foresman, J. Cioslowski, J. V. Ortiz, A. G. Baboul, B. B. Stefanov, G. Liu, A. Liashenko, P. Piskorz, I. Komaromi, R. Gomperts, R. L. Martin, D. J. Fox, T. Keith, M. A. Al-Laham, C. Y. Peng, A. Nanayakkara, C. Gonzalez, M. Challacombe, P. M. W. Gill, B. Johnson, W. Chen, M. W. Wong, J. L. Andres, C. Gonzalez, M. Head-Gordon, E. S. Replogle, J. A. Pople, *Gaussian 98*, Gaussian, Inc., Pittsburgh PA, **1998**.
[54] C. T. Lee, W. T. Yang, R. G. Parr, *Phys. Rev. B* **1988**, *37*, 785–789.
[55] A. D. Becke, *J. Chem. Phys.* **1993**, *98*, 5648–5652.
[56] P. Stephens, F. Devlin, C. Chabalowski, M. Frisch, *J. Phys. Chem.* **1994**, *98*, 11623–11627.
[57] W. R. Wadt, P. J. Hay, *J. Chem. Phys.* **1985**, *82*, 284–298.
[58] P. J. Hay, W. R. Wadt, *J. Chem. Phys.* **1985**, *82*, 299–310.
[59] A. Höllwarth, M. Bohme, S. Dapprich, A. Ehlers, A. Gobbi, V. Jonas, K. Kohler, R. Stegmann, A. Veldkamp, G. Frenking, *Chem. Phys. Lett.* **1993**, *208*, 237–240.
[60] W. Hehre, R. Ditchfie, J. Pople, *J. Chem. Phys.* **1972**, *56*, 2257–2261.
[61] P. Harihara, J. Pople, *Theor. Chim. Acta* **1973**, *28*, 213–222.

Received: May 25, 2008
Published online: September 22, 2008

  